Low-temperature magnetic order rearrangement in the layered van der Waals compound MnPS₃

Sayan Chaudhuri [1] C. N. Kuo,[2,3] Y. S. Chen,[1] C. S. Lue,[2,3] and J. G. Lin[1,4,*]

[1]*Center for Condensed Matter Science, National Taiwan University, Taipei 10617 Taiwan*
[2]*Department of Physics, National Cheng Kung University, Tainan 70101, Taiwan*
[3]*Taiwan Consortium of Emergent Crystalline Materials, Ministry of Science and Technology, Taipei 10622, Taiwan*
[4]*Center of Atomic Initiatives for New Materials, National Taiwan University, Taipei 10617, Taiwan*

To stabilize the long-range magnetic ordering in two-dimensional (2D) materials is a challenge from both fundamental and application points of view. It is difficult to be realized due to the delicate competition between thermal energy, magnetic exchange energy, and spin frustration. Here we study the temperature and field effects on the spin structure of two-dimensional van der Waals system MnPS₃ using dc magnetic susceptibility and electron spin resonance (ESR) techniques. Clear development of three-step transitions was observed in the in-plane susceptibility. A low-temperature plateau from 78 to 38 K can be related to the Heisenberg antiferromagnetic (HAFM) ordering with spins pointing to the z direction. Following, a sharp rising after the plateau suggests a transition into the XY system. The rising slope slows down at 30 K indicating a transition into another phase, possibly a vortex-antivortex state. By fitting the temperature-dependent ESR parameters with the Berezinskii-Kosterlitz-Thouless (BKT) model in the range 100–300 K, we propose a spin 2D system with the vortex-antivortex structure below the HAFM transition. Susceptibility and ESR data show that the application of a high field along the z direction destroys both the XY phase and the BKT transition, reconciling to the scenario of a topological phase transition at zero field.

I. INTRODUCTION

Investigation of 2D materials acquired immense attention recently, owing to their interesting physical properties [1–3] that create tremendous potential applications in the chemical, electrochemical and medical fields. The reduced dimensionality and the interplay between spin, orbital and charge degrees of freedom result into unique phenomena such as superconductivity, multiferroicity, quantum liquid, spin gap-states, chiral phases, etc. [4–6]. The recent success of synthesizing stable 2D materials down to single layer has opened a new era of research [7]. Spin structures in these materials can be manipulated by merely changing the layer numbers, and thus the same material can be implanted easily into various devices with different applications [5]. Although there are numerous examples in the literature for low dimensional magnetic systems, there are only a few that are structurally two dimensional. Most of the known two-dimensional (2D) magnets are structurally 3D systems where the magnetic layers are separated by nonmagnetic layers with weak interlayer coupling, showing a quasi-2D nature [8]. Layered transition metal thiophosphates, MPS₃ (M = first-row transition metals), on the other hand, are in the category of very few compositions, in which both magnetic and crystallographic lattices are 2D. Here, unlike the previous case, the magnetic layers consisting of M atoms are separated by the van der Waals gap. The interplanar M-M distance in MPS₃ is around three times the

in-plane M-M distance so that the interlayer magnetic interactions are very weak. Hence these compositions are known as nearly perfect 2D materials. A schematic crystal structure with space group $C2/m$ is shown from the top and side view in Fig. 1. The M atoms form a honeycomb structure and each M is surrounded by six S atoms with a trigonal symmetry to create the MS₆ octahedra [9]. S atoms are connected to two P atoms above and below the M atom plane. MPS₃ are antiferromagnetic (AFM) and thus can be used in new generation spintronic devices such as ultrafast spin dynamics, with large magnetoresistance effects without any stray field [10]. Moreover, their band gap can be modulated within the range 1.5–3.5 eV by element selection at the M site. The magnetic coupling in these compositions is mainly governed by superexchange interaction, which depends on the M-S-M angle and the d orbital of the metal ion. The MS₆ octahedra give rise to the anisotropic term, which in turn produces different spin dimensionality like Heisenberg with XY of Ising type. The Ising model constrains spins with two directions only, pointing up or down. The XY model confines spin within the xy plane, while in the Heisenberg model the spins can be oriented along any direction.

MnPS₃, a member of this family, has 2D Heisenberg antiferromagnetic (HAFM) structure [8]. It is scientifically interesting because of the symmetry breaking and ferrotoroidicity [11]. According to the Mermin-Wagner (MW) theorem, magnetic ordering cannot occur in 1D or 2D isotropic Heisenberg systems at nonzero temperatures [12], in contrast with the spin system of MnPS₃ that orders antiferromagnetically at 78 K and forms a XY system below 55 K

*Corresponding author: jglin@ntu.edu.tw

[13,14]. MnPS$_3$ orders antiferromagnetically as a result of weak interlayer coupling and it transforms into a XY system at low temperature due to a strong in-plane anisotropy. Precisely speaking, it is an anisotropic Heisenberg system with xy anisotropy. Although the XY system lacks long-range magnetic ordering in MW theory, a topological phase transition might take place at finite temperature due to the binding of magnetic vortex-antivortex pairs, the so-called Berezinskii-Kosterlitz-Thouless (BKT) transition [15]. In the presence of exchange anisotropy and when the spin degrees of freedom are completely reduced from three to two dimensions, the spins can order even without the presence of 3D interaction below the BKT transition temperature. This very unique ordering of spin moments is characterized by an upturn in magnetic susceptibility without any spontaneous magnetization and it has been observed in some specific systems, such as heterogeneous structures, trapped atomic gases, and layered magnetic systems [16–18]. The evidence of xy anisotropy and signature of BKT transition below 50 K in MnPS$_3$ has been shown with the pair-correlation-function analysis [19].

Electron spin resonance (ESR) is a sensitive probe for spin structure and spin dynamics. The temperature and angular dependencies of the ESR spectral parameters can provide critical information for complex spin interactions, such as the BKT correlations in Bi$_{0.5}$Sr$_{0.5}$Mn$_{0.9}$Cr$_{0.1}$O$_3$ [20] and CrBr$_3$ [21]. Early ESR study on MnPS$_3$ [22] confirmed its antiferromagnetic nature below 78 K. After the discovery of its XY-like state at low temperature [13,19], there is no thorough magnetic and ESR study on the light of magnetic transition from different phases. In this work, we observe a three step transition from Heisenberg to XY and to BKT transition in susceptibility data. Further, the temperature and angular dependencies of the ESR linewidth are analyzed in the temperature range 100–300 K. The linewidth as a function of temperature follows the BKT transition model satisfactorily, while the extracted critical parameter from fitting to Ginzberg-Landau critical model confirms a 2D correlation. Overall, we provide a clear explanation for the temperature evolution of spin structure in MnPS$_3$, which advances the knowledge of spin ordering in 2D materials.

II. EXPERIMENTAL DETAILS

The flakelike MnPS$_3$ single crystal was synthesized using the chemical vapor deposition technique. Primary structural characterization was done using x-ray diffraction (XRD) at room temperature. To confirm the phase formation, room temperature Raman spectra were recorded with the incident laser beam energy being kept below 50 mW to prevent local heating. The dc magnetic susceptibility was measured as a function of temperature and field using a Quantum Design MPMS system. The samples were encapsulated inside a plastic straw and placed in the center of the magnetic field. For the ESR measurements, the encapsulated samples were placed at the center of a TE$_{102}$ cavity, connected to a microwave generator and a lock-in amplifier to derive the field first derivative of the absorbed power. The microwave source is provided by Bruker EMX system with a fixed frequency of 9.4 GHz. During ESR measurement, the external magnetic field H was applied either parallel to the sample surface or rotating in the
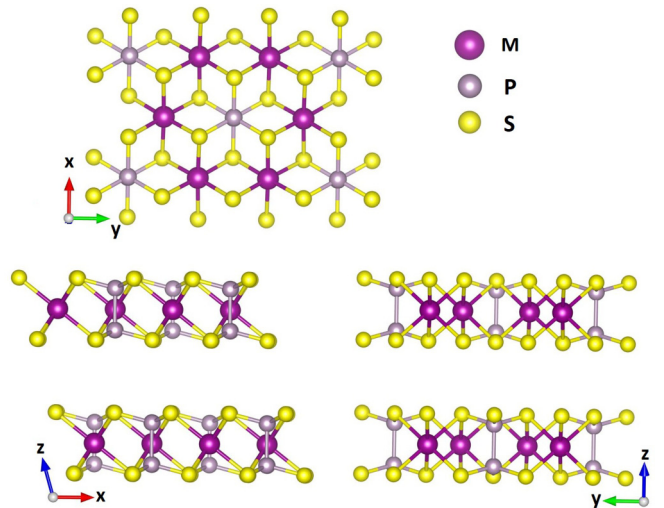

FIG. 1. Schematic structure of MPS$_3$ system viewed from different axis directions.

out-of-plane direction with respect to the sample surface. A liquid N$_2$ cryostat was used to record the ESR spectra down to 100 K.

III. RESULTS AND DISCUSSION

Figure 2(a) shows the XRD pattern of MnPS$_3$ crystal. The presence of major peaks (001), (002), and (003) reveals a formation of pure monoclinic phase [23]. There is no trace of any other peak from a second phase. Raman spectra are shown in Fig. 2(b) with the characteristic vibration modes denoted as P_i ($i = 1–7$), consistent with previously reported results [13,24]. Thus, it confirms that we have synthesized a high-quality single crystal of MnPS$_3$.
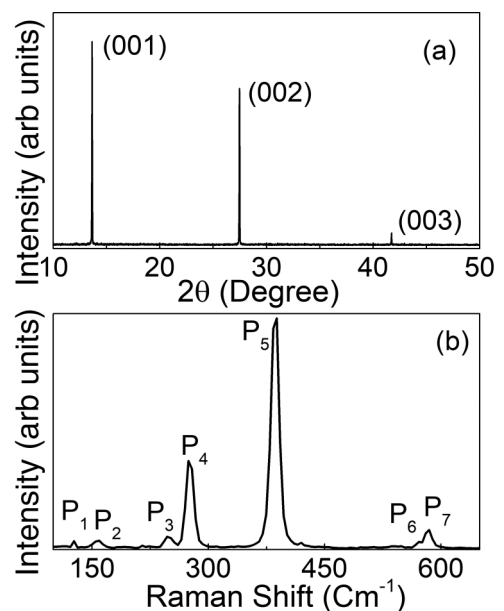

FIG. 2. (a) XRD profile of single crystalline MnPS$_3$; (b) room temperature Raman spectra for MnPS$_3$.
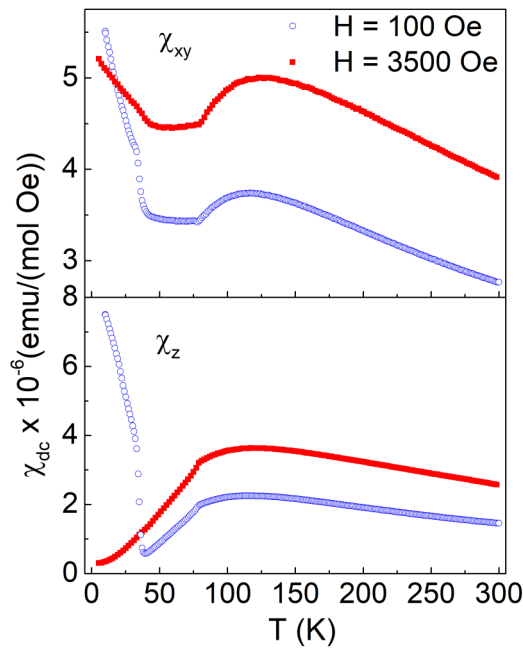
FIG. 3. Magnetic susceptibility of MnPS$_3$ single crystals perpendicular (top panel) and parallel (bottom panel) to the c axis.

FIG. 4. Magnetization isotherms of MnPS$_3$ at 5 K.

Figures 3(a) and 3(b) display the temperature dependencies of dc susceptibilities (χ_{dc}) with a zero-field-cooled (ZFC) mode for two directions of magnetic fields, in-plane (χ_{xy}) and out-of-plane (χ_z). The data measured at low field (100 Oe) and high field (3500 Oe) are denoted by open circles and closed squares respectively. In general, the broad maximum around 120 K follows the picture of critical fluctuation in a low dimensional magnet with short spin-spin correlation [8]. Below the broad maximum, we obtain a shallow plateau region followed by a sharp upturn in susceptibility. The upturn is absent when high magnetic field is applied in the out-of-plane direction.

The magnetic behavior of the MnPS$_3$ below the antiferromagnetic transition is much debated in the literature. As discussed earlier in the text, the plateau region has been explained with a MFA model and the upturn in χ_{xy} as a contribution from spin waves [8,25].

In the present study, we observe three transitions in the χ_{xy} data at 100 Oe, which can be identified as the following: The paramagnetic state to HAFM transition at $T_N \sim 78$ K (the onset of plateau), the HAFM to XY transition at 38 K (the end of the plateau), and a possible topological order at $\sim$30 K (first upturn). The constant χ_{xy} between 78 and 38 K was predicted by the mean-field approximation (MFA) model for a magnetic field applied perpendicular to the spin moments (in-plane field direction in HAFM) [8]. The sharp upturn of χ_{xy} indicates the spin switching from the z direction to the xy plane, which was absent in previous χ_{xy} reports on MnPS$_3$ [25]. As to the second upturn with a smaller slope, it is possibly a BKT transition which has been proposed from the Neutron experiment [19]. The curve of χ_{xy} at 3500 Oe has a similar feature compared with that at 100 Oe except shifting upward and the two curves cross over at 25 K. Apparently, the application of 3500 Oe along the xy plane aids the confinement of the spin orientation
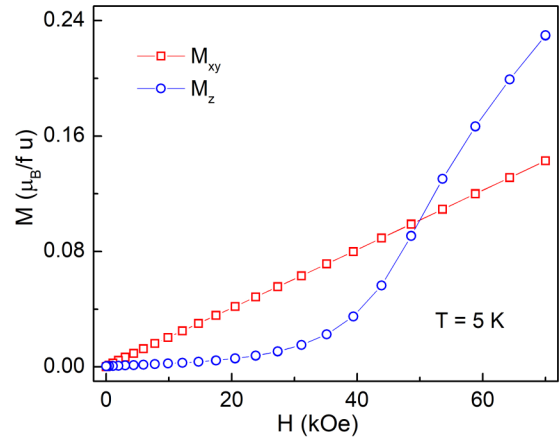
into the xy plane and raises the AFM transition temperature from 78 to 81 K. This could enhance the XY-type behavior comparing to the case at low field as seen from the broadening of the upturn in high field.

On the other hand, the χ_z data at 100 Oe only show two transitions without the plateau. Below T_N the transition from Heisenberg to XY state starts, causing a decrease in the number of spins along the z axis and an increase in that along the xy plane. Near 38 K, the system transits into a purely 2D XY system, i.e., the out-of-plane component of the antiferromagnetic coupling becomes negligible, which gives rise to the upturn in χ_z [18]. At 3500 Oe, the spins orient towards the field direction, thereby diminishing the 2D XY structure. As a result, the upturn in χ_z vanishes.

Magnetization isotherms at 5 K are shown in Fig. 4. The M_z exhibits a huge upturn in magnetization between 40 and 70 kOe, which has been identified as a spin-flop transition [22,26]. The M_{xy} on the other hand shows an almost linear behavior as expected for an antiferromagnetic system having a coherent rotation of magnetic moments. There is no spontaneous magnetization as shown in the figure.

ESR spectra from 300 to 100 K with the applied field perpendicular to the c axis ($\theta = 90°$) are depicted in Fig. 5,
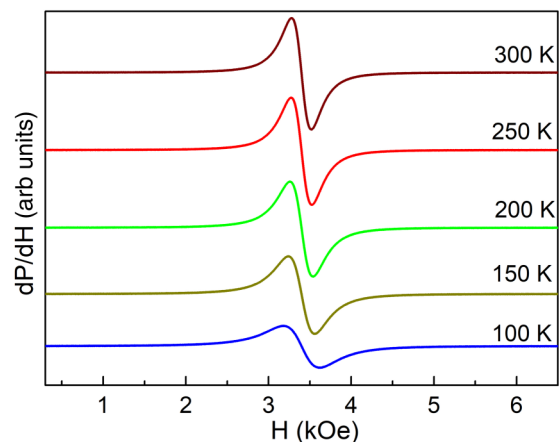

FIG. 5. ESR spectra of single crystalline MnPS$_3$ at various temperatures.
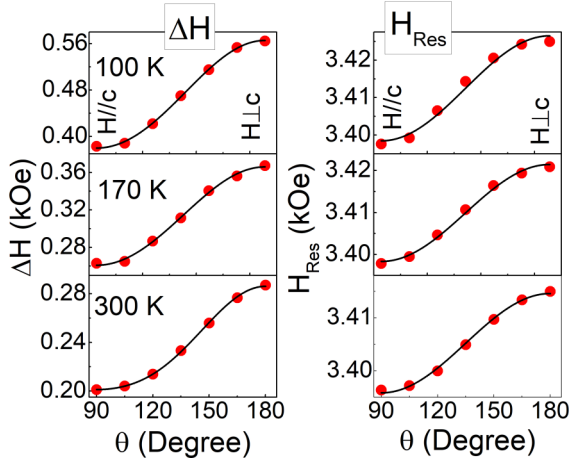
FIG. 6. Angular dependence of ESR linewidth (left column) and resonance field (right column) measured at selected temperatures. The black lines indicate the model fitting.

showing strong and broad absorption lines. The two spectral parameters, resonance field (H_{Res}) and half-width at half maximum linewidth (ΔH), were extracted by fitting the lines with the first derivative of the Lorentzian function. Angular dependent H_{Res} and ΔH were plotted in the left and right columns of Fig. 6 respectively.

The values of ΔH shown in the left panel of Fig. 6 are fitted based on Heisenberg system using the following equation [27]:

$$\Delta H(\theta) = A(3\cos^2\theta - 1)^2 + B\cos^2\theta + C, \qquad (1)$$

where θ is the angle between the c axis and applied field and the $B\cos^2\theta$ term is added to accommodate the higher q, with q being the long-wavelength mode [27]. H_{Res} vs angle were fitted using the following equation:

$$H_{Res}(\theta) = D(3\cos^2\theta - 1) + E. \qquad (2)$$

The extracted fitting parameters of $\Delta H(\theta)$ and $H_{Res}(\theta)$ are summarized in Table I. The $3\cos^2\theta - 1$ behavior of H_{Res} is a characteristic of 2D spin systems irrespective of their crystal structure, and can be explained as a result of noncubic distribution of dipoles in a 2D lattice. Similar results were found in many other 2D systems, such as K_2MnF_4 [28], K_2CuF_4 [29], $CrCl_3$ [30], and $CrBr_3$ [21]. As can be noticed from Table I, both anisotropy parameters (A and D) increase with decreasing temperature, indicating the enhancement of magnetic ordering. Simultaneously the value of the B parameter increases, which hints of an increment of contribution from higher q modes as expected in the 2D HAFM systems.

The variations of H_{Res} and ΔH as a function of temperature with field parallel to the xy plane and z axis are shown in

FIG. 7. BKT and critical model fits for ESR linewidth when magnetic field applied (a) parallel to the xy plane and (b) z axis. The inset shows the quality of the BKT fit using logarithmic plot $\ln(\Delta H)$ vs the reduced temperature $-(T/T_{BKT} - 1)^{-0.5}$. The corresponding real temperature values are shown in the upper x axis of the inset.

Figs. 7(a) and 7(b) respectively. The temperature dependence of ΔH above the magnetic transition generally follows the Ginzberg-Landau (GL) critical model [20],

$$\Delta H = \frac{K}{\left(\frac{T}{T_N} - 1\right)^p} + mT + \Delta H_0, \qquad (3)$$

with K being a constant and p the critical exponent. p is between 0.5 and 0.7 for a 2D HAFM system [30]. The linear coefficients (m and ΔH_0) are added to the equation to describe the physics at the complete paramagnetic phase of the system. The solid blue curve in Fig. 7 represents the least square fitting to the GL critical model and the extracted fitting parameters for the $H//xy$ plane are summarized in Table II. The extracted values of m and ΔH_0 are very small, indicating that a purely paramagnetic phase does not exist within the temperature range. $p = 0.3$ is less than the theoretical value for a 2D HAFM system but close to that for a 2D XY system.

TABLE I. Fitting parameters for the angular dependent ESR data.

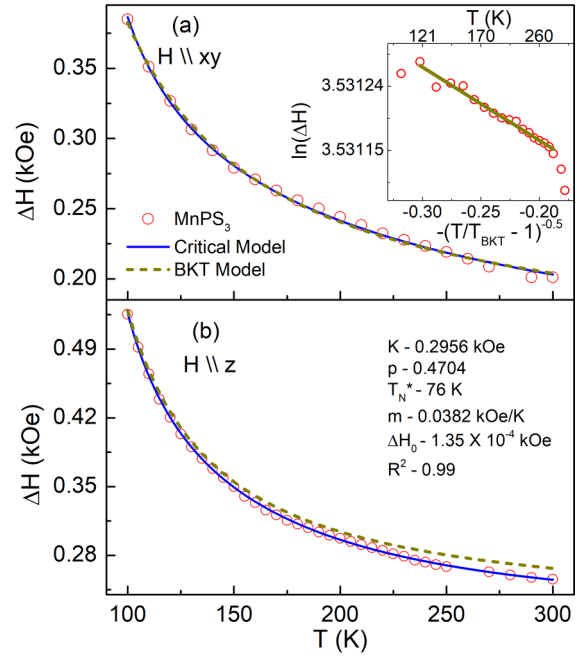| T (K)	A (kOe)	B (kOe)	C (kOe)	D (kOe)	E (kOe)
100	0.0062	0.1797	0.3779	0.0094	3.4078
170	0.0055	0.1031	0.2603	0.0077	3.406
300	0.005	0.0698	0.1962	0.0063	3.4021

TABLE II. Summary of fit parameters and goodness of fit for critical and BKT model. The starred parameters were constrained to within the range of physically or experimentally known values.

Critical model fitting		BKT model fitting	
Parameters	Extracted values	Parameters	Extracted values
K (kOe)	0.279	ΔH_∞ (kOe)	0.042
P	0.311	b*	$\pi/2$
T_N (K)*	78	T_{BKT} (K)	9.7
m (kOe/K)	8.29×10^{-27}	m (kOe/K)	7.5×10^{-65}
ΔH_0 (kOe)	0.0036	ΔH_0 (kOe)	0.0081

However, the critical model fits well to the data for $H//z$ axis with a critical exponent $p = 0.47$, which is very close to the value for the 2D HAFM system. Next, we fit the ΔH using the BKT model [17], where

$$\Delta H = \Delta H_\infty \exp\left[\frac{3b}{\sqrt{\frac{T}{T_{\mathrm{BKT}}} - 1}}\right] + mT + \Delta H_0. \quad (4)$$

ΔH_∞ represents the linewidth at infinite temperature and T_{BKT} is the characteristic BKT transition temperature. The value of b is taken as $\pi/2$ [20]. The fitting results show that the BKT model fits well the behavior of $\Delta H(T)$ with $H \backslash\backslash xy$ but it does not fit well with the $\Delta H(T)$ with $H \backslash\backslash z$. The quality of the BKT fit using logarithmic plot $\ln(\Delta H)$ vs the reduced temperature $-(T/T_{\mathrm{BKT}} - 1)^{-0.5}$ is shown in the inset of Fig. 7(a). Linear behavior of the plot confirms the BKT-like transition in the system. This result signifies that the BKT transition (and the XY system) is destroyed by the field applied perpendicular to the sample surface during the ESR measurement, which is consistent with the high field data of χ_z. The ratio of $T_{\mathrm{BKT}}/T_{\mathrm{N}}$ is small compared to other systems showing BKT transition [31] and rather close to the systems having field induced BKT transition [20,21]. A detailed understanding of the magnetic dynamics needs further experimental evaluation at low temperatures. The field dependence of transition as seen in our experiments confirms the BKT transition and also provides a route to tune different magnetic phases in the 2D system for future applications of spintronic devices.

IV. CONCLUSION

In conclusion, we investigated the nature of magnetic transitions for a 2D van der Walls antiferromagnetic system MnPS$_3$ using dc magnetic susceptibility χ_{dc} and ESR techniques, and with the applied field along two different directions, the xy plane and the z direction. Based on the analysis of χ_{xy} and χ_z, the MnPS$_3$ transits from paramagnetic to Heisenberg antiferromagnetic state at 78 K, and then to the XY phase at around 38 K. The XY phase of the system is prone under 3500 Oe field applied parallel to the xy direction but suppressed completely when the field is along the z axis. Further, the theoretical fitting on the temperature-dependent ESR linewidth shows that the BKT correlation exists with the field along the xy plane but not with the field along the z direction. The temperature and field dependencies of magnetic transitions provide clear evidence for the evolution of spin structure from HAFM to XY and to the vortex-antivortex state in MnPS$_3$.

[1] Y. Tian, M. J. Gray, H. Ji, R. J. Cava, and K. S. Burch, 2D Mater. **3**, 025035 (2016).

[2] M. W. Lin, H. L. Zhuang, J. Yan, T. Z. Ward, A. A. Puretzky, C. M. Rouleau, Z. Gai, L. Liang, V. Meunier, B. G. Sumpter, P. Ganesh, P. R. C. Kent, D. B. Geohegan, D. G. Mandrus, and K. Xiao, J. Mater. Chem. C **4**, 315 (2016).

[3] X. Zhang, X. Zhao, D. Wu, Y. Jing, and Z. Zhou, Adv. Sci. **3**, 1600062 (2016).

[4] W. Wang, M. W. Daniels, Z. Liao, Y. Zhao, J. Wang, G. Koster, G. Rijnders, C. Z. Chang, D. Xiao, and W. Wu, Nat. Mater. **18**, 1054 (2019).

[5] B. Huang, G. Clark, E. Navarro-Moratalla, D. R. Klein, R. Cheng, K. L. Seyler, Di. Zhong, E. Schmidgall, M. A. McGuire, D. H. Cobden, W. Yao, D. Xiao, P. Jarillo-Herrero, and X. Xu, Nature (London) **546**, 270 (2017).

[6] S. Kezilebieke, M. N. Huda, V. Vaňo, M. Aapro, S. C. Ganguli, O. J. Silveira, S. Głodzik, A. S. Foster, T. Ojanen, and P. Liljeroth, Nature (London) **588**, 424 (2020).

[7] M. Bonilla, S. Kolekar, Y. Ma, H. C. Diaz, V. Kalappattil, R. Das, T. Eggers, H. R. Gutierrez, M. H. Phan, and M. Batzill, Nat. Nanotechnol. **13**, 289 (2018).

[8] P. A. Joy and S. Vasudevan, Phys. Rev. B **46**, 5425 (1992).

[9] J. U. Lee, S. Lee, J. H. Ryoo, S. Kang, T. Y. Kim, P. Kim, C. H. Park, J. G. Park, and H. Cheong, Nano Lett. **16**, 7433 (2016).

[10] V. Baltz, A. Manchon, M. Tsoi, T. Moriyama, T. Ono, and Y. Tserkovnyak, Rev. Mod. Phys. **90**, 015005 (2018).

[11] E. Ressouche, M. Loire, V. Simonet, R. Ballou, A. Stunault, and A. Wildes, Phys. Rev. B **82**, 100408(R) (2010).

[12] N. D. Mermin and H. Wagner, Phys. Rev. Lett. **17**, 1133 (1966).

[13] Y. J. Sun, Q. H. Tan, X. L. Liu, Y. F. Gao, and J. Zhang, J. Phys. Chem. Lett. **10**, 3087 (2019).

[14] A. R. Wildes, H. M. Rønnow, B. Roessli, M. J. Harris, and K. W. Godfrey, Phys. Rev. B **74**, 094422 (2006).

[15] J. M. Kosterlitz and D. J. Thouless, J. Phys. C: Solid State Phys. **6**, 1181 (1973).

[16] Z. Hadzibabic, P. Krüger, M. Cheneau, B. Battelier, and J. Dalibard, Nature (London) **441**, 1118 (2006).

[17] M. Heinrich, H.-A. Krug von Nidda, A. Loidl, N. Rogado, and R. J. Cava, Phys. Rev. Lett. **91**, 137601 (2003).

[18] A. Cuccoli, T. Roscilde, R. Vaia, and P. Verrucchi, Phys. Rev. Lett. **90**, 167205 (2003).

[19] H. M. Rønnow, A. R. Wildes, and S. T. Bramwell, Phys. B (Amsterdam, Neth.) **276–278**, 676 (2000).

[20] A. Ashoka, K. S. Bhagyashree, and S. v. Bhat, Phys. Rev. B **102**, 024429 (2020).

[21] C. L. Saiz, J. A. Delgado, J. van Tol, T. Tartaglia, F. Tafti, and S. R. Singamaneni, J. Appl. Phys. **129**, 233902 (2021).

[22] K. Okuda, K. Kurosawa, S. Saito, M. Honda, Z. Yu, and M. Date, J. Phys. Soc. Jpn. **55**, 4456 (1986).

[23] Z. Ur Rehman, Z. Muhammad, O. A. Moses, W. Zhu, C. Wu, Q. He, M. Habib, and L. Song, Micromachines **9**, 292 (2018).

[24] F. Kargar, E. A. Coleman, S. Ghosh, J. Lee, M. J. Gomez, Y. Liu, A. S. Magana, Z. Barani, A. Mohammadzadeh, B. Debnath, R. B. Wilson, R. K. Lake, and A. A. Balandin, ACS Nano **14**, 2424 (2020).

[25] G. Long, T. Zhang, X. Cai, J. Hu, C. W. Cho, S. Xu, J. Shen, Z. Wu, T. Han, J. Lin, J. Wang, Y. Cai, R. Lortz, Z. Mao, and N. Wang, ACS Nano **11**, 11330 (2017).

[26] D. J. Goossens, A. R. Wildes, C. Ritter, and T. J. Hicks, J. Phys.: Condens. Matter **12**, 1845 (2000).

[27] S. Chehab, J. Amiell, P. Biensan, and S. Flandrois, Physica B (Amsterdam, Neth.) **173**, 211 (1991).

[28] K. Nagata, I. Yamamoto, H. Takano, and Y. Yokozawa, J. Phys. Soc. Jpn. **43**, 857 (1977).

[29] I. Yamada, I. Morishita, and T. Tokuyama, Physica B+C (Amsterdam) **115**, 179 (1983).

[30] H. Benner and J. P. Boucher, Phys. Chem. Mater. Low-Dimens. Struct. **9**, 323 (1990)).

[31] M. Hemmida, N. Winterhalter-Stocker, D. Ehlers, H.-A. Krug von Nidda, M. Yao, J. Bannies, E. D. L. Rienks, R. Kurleto, C. Felser, B. Büchner *et al.*, Phys. Rev. B **103**, 195112 (2021).